Electrocatalysis (2023) 14:202–212
https://doi.org/10.1007/s12678-022-00787-7

RESEARCH

Physical and Electrochemical Effect of Bimetallic Pd–Mo Nanoalloys Supported on Vulcan XC-72R Carbon as Cathode Catalysts for Proton Exchange Membrane Fuel Cell

Ömer Şahin[1] · **Abdurrahman Akdağ**[2] · **Sabit Horoz**[3] · **Arzu Ekinci**[4]

Accepted: 19 October 2022 / Published online: 28 October 2022

Abstract

Synthesis of the bimetallic carbon-supported Pd and PdMo electrocatalysts via the chemical reduction with sodium borohydride as a reducing agent is presented. The Pd/C and PdMo/C electrocatalysts were used as cathode electrocatalysts in proton exchange membrane (PEM) fuel cells in order to examine their catalytic activity. The characterization of the prepared nanoparticles has been carried out using various methods, including X-ray diffraction (XRD), scanning electron microscopy (SEM), and energy- dispersive X-ray analysis (EDX). Moreover, the activities of the produced catalysts have been determined using cyclic voltammetry (CV), chronoamperometry, electrochemical impedance spectroscopy (EIS), and single-cell PEM fuel cell. The findings reveal that the crystallite size of the electrocatalysts Pd and Pd–Mo is less than 5.5 nm and that the Pd–Mo/C catalyst exhibits high activity for the oxygen reduction process when used alone. Furthermore, catalysts outperform other temperatures at 70 °C under varied cell temperatures and Mo concentrations in a single-cell fuel cell. A single cell using Pd–Mo/C as the cathode achieves a maximum power density of 107 mW cm^{-2} at its maximum current density. Maximum current densities of synthesized catalysts at 70 °C cell temperature were measured as 61, 116, 188, and 168 mA cm^{-2} for Pd/C, PdMo/C, $PdMo_2$/C, and $PdMo_3$/C catalysts, respectively. The efficiency according to the current of the $PdMo_2$/C cathode catalyst at 70 °C was 52%, and Pd/C, PdMo/C, and $PdMo_3$/C cathode catalysts at the same temperature were calculated as 26%, 38%, and 50%, respectively. The evenly scattered nanoparticles and more crystalline lattice flaws in the Pd–Mo/C catalyst are thought to be responsible for the catalyst's superior performance.

Keywords Proton exchange membrane fuel cells · Palladium molybdenum catalyst · Oxygen reduction reaction · Electro catalyst

✉ Arzu Ekinci
aekinci@siirt.edu.tr

Ömer Şahin
omersahin@itü.edu.tr

Abdurrahman Akdağ
aakdag@harran.edu.tr

Sabit Horoz
sabit.horoz@sivas.edu.tr

[1] Department of Chemical Engineering, Faculty of Engineering, Istanbul Technical University, Istanbul, Turkey

[2] Department of Medical Laboratory Techniques, Vocational School of Health Services, Harran University, Sanliurfa, Turkey

[3] Metallurgical and Materials Engineering, Sivas Science and Technology University, Sivas, Turkey

[4] Department of Occupational Health and Safety, Faculty of Health Sciences, Siirt University, Siirt, Turkey

Introduction

Proton exchange membrane (PEM) fuel cells operating at low temperatures and high power densities are considered one of the most promising technologies for clean energy devices capable of producing efficient and environmentally friendly energy, along with the implementation of sustainable development concepts in the energy industry [1–3]. Because of their high power density and versatility, PEM fuel cells have received much attention over the last few decades [4–6]. However, owing to the use of platinum (Pt) metal and the slow kinetics of the ORR on the cathode side, PEM fuel cells are presently constrained by their expensive cost [7–9]. As a result, an acidic electrolyte catalyst with high activity in a non-platinum environment is urgently needed. Because palladium and platinum have similar valence electronic configurations and lattice constants [10, 11], researchers have focused on the development of palladium-based catalyst materials for the oxygen reduction reaction (ORR) in PEM fuel cells and DMFCs (direct methanol fuel cells) [12–15]. The palladium and palladium-based alloys have shown strong activity in the electro-oxidation of alcohols in alkaline environments, making them viable alternatives to platinum [16–21]. Searching for appropriate support materials in the realm of heterogeneous catalysis is another effective technique for minimizing noble metal loading and improving catalyst performance. As electrocatalyst supports, carbon materials with diverse structures and forms, such as active carbon, carbon nanofibers, and carbon nanotubes, have been employed [22–24]. Other than carbon, no other material has the necessary attributes for the commercialization of fuel cells, such as corrosion resistance, electronic conductivity, and low cost. Compared to other conductive carbon black grades, Vulcan XC-72R carbon black (VC) may give high conductivity at low loading levels while also being simpler to disseminate throughout the surface [24]. The production of Pd nanoparticles with homogeneous dispersion has taken effort [10, 25–28]. However, no reports of the Pd–Mo bimetallic catalysts for PEM electro-oxidation have been published to the best of our knowledge. In particular, in this research, less-costly carbon Vulcan XC-72-supported Pd–Mo nanoparticles are synthesized by chemical reduction using sodium borohydride and formic acid methods as electro-catalysts in PEM fuel cells.

The characterization and electrochemical activity measurements of the $PdMo_2/C$ catalyst with a 1:2 atomic ratio of Pd: Mo, which showed the best activity in the PEM fuel cell test study, were performed. The structural characteristics of the materials are researched using X-ray diffraction (XRD), a scanning electron microscope (SEM), and the energy dispersion spectrometer (EDX) mapping. Electrochemical activities of the catalyst are determined by electrochemical surface area (ECSA), cyclic voltammetry (CV), and electrochemical impedance spectroscopy (EIS) determined by alternating current impedance measurements. Different ratios of the PdMo/C catalyst cathode, including MEA with a 1 cm^2 active area, are tested at four different temperatures (40 °C, 50 °C, 60 °C, and 70 °C) in the presence of supplied humidified H_2/O_2 gases.

Material and Methods

Chemicals

A variety of substances were used in the present investigation. The compounds are described below.

Sodium borohydride ($NaBH_4$, 99%), ethanol (99.9%), formic acid (HCOOH, $\geq$98%), isopropyl alcohol, and Nafion solution (5% dispersion) were purchased from Aldrich; palladium(II) chloride ($PdCI_4$, 98%) and ammonium molybdate tetrahydrate ($(NH_4)_6Mo_7O_{24}·4H_2O$) were bought from Sigma Aldrich and they were used. Vulcan XC-72R carbon powder carbon black is acquired from Cabot. Electrochem Inc. provided the other materials used, including Nafion TM 117 membranes and Teflon TM processed by Toray TM carbon paper, which is purchased from the fuel cell store.

Synthesis of Catalyst

PdMox/C (x:1, 2, 3) catalysts were prepared by the chemical reduction method. The platinum chloride and ammonium molybdate tetrahydrate were used as metal precursors and sodium borohydride and formic acid as reducing agents. All of the catalysts were produced with a metal loading to support 20 wt%. All catalysts synthesized in different ratios of Pd:Mo (1:1, 1:2, and 1:3 molar ratios) were prepared. The proper quantity of carbon (Vulcan XC-72) was then dispersed in 10 ml ethyl alcohol for 1 h using a magnetic mixer. Next, the platinum chloride and ammonium molybdate tetrahydrate were added to the solution and homogenized using an ultrasonic mixer for 30 min. Before the reduction process, to prevent it from reacting with water instead of metal salts of sodium boron hydride added, the pH of the catalyst of the compound was adjusted to pH 11 by adding 0.5 M NaOH, and the solution was heated until the temperature reached 80 °C. Next, the 10 ml $NaBH_4$ and 5 ml of formic acid solutions were dropped slowly, and the reduction process was carried out at a solution temperature of 80 °C. The resulting suspension was filtered, and the obtained sediment was dried in a drying oven at 110 °C in a nitrogen gas medium for 5 h. The Pd/C catalyst was likewise synthesized using the same process as described above.

Preparation of the MEA and Fuel Cell Testing

MEAs are traditionally manufactured by two methods, the membrane-based method or the GDL-based method [29]. In the GDL-based method, a catalyst layer is applied onto one side of the GDL forming a catalyst-coated GDL (CCG) [30]. The gas diffusion layer (GDL)-based technique created was employed to create the MEAs (1 cm^2 active area) used in this investigation. The concentration of 20% PdMox alloys was utilized as a catalyst in the cathode electrode. In the PdMo/C catalyst, 0.13 mg(Pd) cm^{-2} was used; in the $PdMo_2/C$ catalyst, 0.096 mg(Pd) cm^{-2} was used; and in the $PdMo_3/C$ catalyst, 0.072 mg(Pd) cm^{-2} was used.

The catalyst and the 5 wt.% Nafion ionomer solution was combined with an isopropanol solution to generate a homogenous catalyst suspension for use as the cathode in the electrochemical cell. The catalyst inks were painted onto the GDLs with a 0.15 mg(Pt) cm^{-2} metal loading for anode electrodes. For the gas diffusion layer, carbon cloth (Toray TM, no metal) and the solid electrolyte membrane were used on Nafion 117. Anode and cathode diffusion layers were prepared by hot pressing MEAs on Nafion membrane-117 at 135 °C and 65 kgcm^{-2} pressure for 3 min.

The anode side is tested with 50% humidified H_2 gas and the cathode side is tested with 50% O_2 gas. H_2 and O_2 gases had a flow speed of 20 ml dk^{-1}, and the fuel cell had a working temperature of 40, 50, 60, and 70 °C. To get the best performance out of each MEA, polarization curves were taken and activated at 0.6 V until stable results were found. The humidification and cell temperatures were set for 30 min, and then nitrogen was delivered to the anode and cathode sides [31]. The maximum power output was then repeated at that level until no more variation was seen. After the fuel cell had reached the desired temperatures, hydrogen and oxygen were introduced [2, 32].

Characterization of the Catalyst Materials

XRD (Rigaku X-ray diffractometer) and SEM, EDX (JEOL JSM 6610) measurements were carried out to examine the structural and morphological properties of Pd/C and $PdMo_2/C$ catalysts.

Electrochemical Measurements

For electrochemical measurements, cyclic voltammetry, chronoamperometry, and electrochemical impedance spectroscopy techniques were used. Measurements were taken in a 0.5 M H_2SO_4 solution. For electrochemical tests, CHI 660E equipment was employed. The working electrode was a glassy carbon electrode with a diameter of 3 mm, the reference electrode was Ag/AgCl (3 M, KCl), and the counterelectrode was a platinum (Pt) plate. The CV voltammetry measurements were taken in the potential range of $-0.3/1.2$ V. Chronoamperometry measurements were performed at -0.1 V. In this experiment, alternating current impedance measurements were taken at a potential of 0.5 V in the frequency range from 10^{+5} to 10^{+2} Hz. An ultrasonic bath was used to sonicate 5 mg of catalyst in a combination of 960 ml of ethanol and 40 µl of Nafion solution (5%), which was then left to stand for 30 min to conduct electrochemical tests. Then, 2 µl of the mixture was applied to the glassy carbon electrode surface using a micropipette, and measurements were performed when the mixture had dried completely.

Results and Discussions

The Results of Physical Characterization

Figure 1 shows the XRD patterns of the $PdMo_2/C$ catalyst with the Pd:Mo (1:2) ratio determined as the best Mo ratio and the Pd/C catalyst for comparison. The Pd/C patterns are seen a broad peak at $2\theta = 24.96$, attributed to the (200) plane of the carbon support, and a succession of peaks at $2\theta = 40.18°$, 46.03°, and 68.20°, respectively. The single cubic fcc phase of palladium is defined by its peaks, which are attributed to planes (111), (200), and (220). The experimental pattern corresponds to JCPDS card 01–087-0643 [10], containing conventional crystallographic tables. Despite the similarity in the patterns of the Pd/C and Pd/Mo samples, the addition of Mo causes the peaks to be slightly moved to higher values of 2θ, which suggests a contraction of the lattice and the production of alloy [33, 34]. The absence of any Mo element or compound peak in the XRD patterns for PdMo phases indicates that the samples are independent of visible phase segregation [35]. The EDX spectra of the PdMo/C catalyst, on the other hand, unambiguously demonstrate the presence of Mo (Fig. 2). Scherrer's equation is employed to calculate the average crystallite size for the catalysts based on the (111) diffraction peak seen.

$$d = 0.9\lambda/(\beta\cos\theta) \quad (1)$$

β is the width of the peak obtained as a result of x-ray diffraction, d is the crystal size, λ is the wavelength of the x-ray used, and θ is the Bragg angle at which the plane is observed. The average crystallite sizes calculated for the Pd/C and $PdMo_2/C$ catalysts are 5.13 and 4.66 nm, respectively.

SEM imaging was used to examine the morphology of Pd/Mo and $PdMo_2/C$ catalysts (Fig. 2a and b). The well-controlled and homogeneous nucleation and growth caused by sodium borohydride and formic acid as reducing agents might be ascribed to the Pd/C and $PdMo_2/C$ catalyst advantageous morphology. In the pictures, the visible white spots are thought to represent a

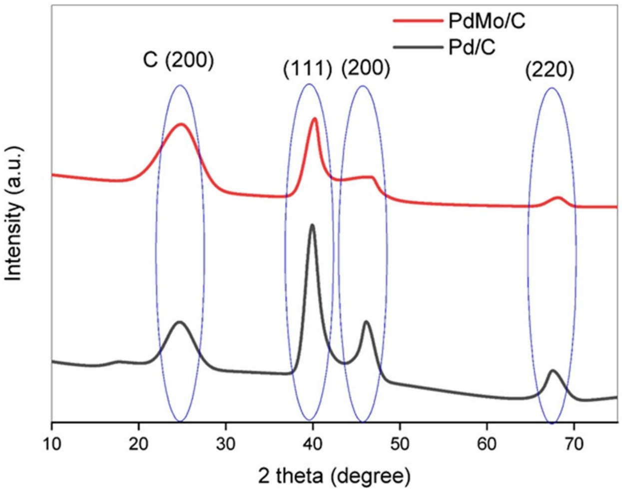

Fig. 1 XRD results of Pd/C and $PdMo_2/C$ catalysts

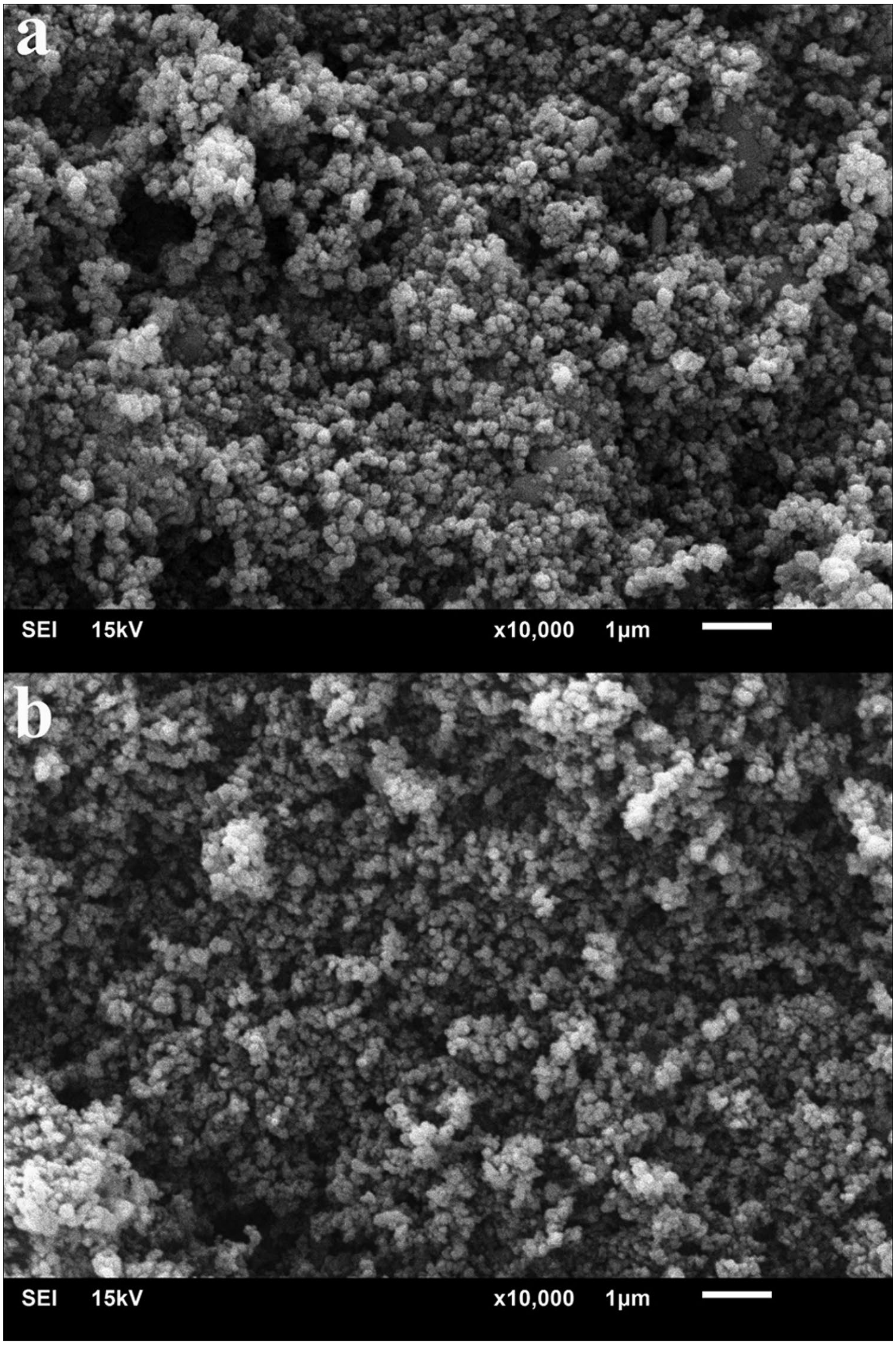

Fig. 2 SEM imagines of **a** Pd/C and **b** $PdMo_2/C$

rough surface covered with agglomerates of well-defined spherical palladium particles deposited in the presence of a Vulcan carbon substrate with a dense and particulate structure. However, energy dispersive X-ray spectroscopy (EDX) analysis on the samples was carried out to collect the requisite experimental proof of the catalyst on the support.

The EDX analysis shown in Fig. 3a, b for the Pd/C and $PdMo_2/C$ catalysts clearly shows that bimetallic nanomaterials of Pd and Mo are formed. The mean atomic percentages for Mo and Pd, according to the EDX study, were 6.1% and 9.6%, respectively.

In the molybdenum-rich $PdMo_2$ catalyst, a typical signal of Mo (Lα) at 2.18 keV was observed [36, 37]. In addition, the

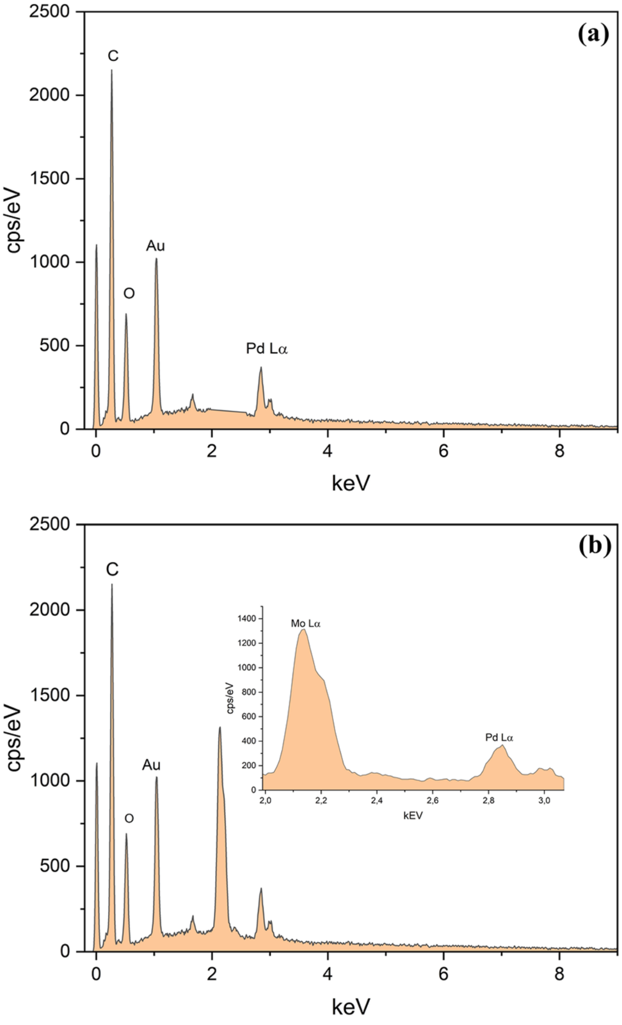

Fig. 3 EDX spectrum of catalysts **a** Pd/C and **b** $PdMo_2/C$

energy peak of Pd (Lα) was also observed at 2.85 keV [38]. In addition, a low divergence between Pd and Mo atomic ratios is available, indicating a uniform composition. EDX element mapping shows the homogeneous distribution of palladium and molybdenum along the metal line (Fig. 4a, b).

Electrochemical Measurements

Cyclic Voltammetry

Cyclic voltammograms of the Pd/C and $PdMo_2/C$ catalysts were studied in a 0.5 M H_2SO_4 solution, as shown in Fig. 5. The electrochemical behaviors of Pd-based nanomaterials are shown in these voltammograms. The adsorption/desorption of the H on the catalyst surface was attributed to the observed peaks in the CV potential range of − 0.25 to 0.10 V. The size of these peaks is related to the electrochemically active surface area of Pt. However, because of the hydrogen-absorbing characteristic of Pd, the size of the electrochemically active surface area determined by this approach does not entirely correspond to the absolute values [39, 40], as previously stated. As a result, it is easy to compute Pd's electrochemically active surface area, which is determined by the charge in the PdO reduction peaks [41], which is the most convenient method. The upper potential limit for the creation of PdO monolayers, on the other hand, should be well established. Finally, the amount of charge passed for the PdO reduction peaks in the CVs obtained by determining different upper potential limits is determined. Charge values displayed as a function of the upper potential limit reveal that the coordinates at the point at which the line changes its slope correspond to a whole PdO monolayer development [42]. According to the results of the measurements, the top potential limit was determined to be 1.4 V.

In cathodic scanning, the PdO reduction peaks are around 0.44 and 0.41 V for Pd/C and $PdMo_2/C$, respectively. It was observed that the peak for $PdMo_2/C$ is the largest of these peaks. This shows that the $PdMo_2/C$ catalyst has a greater surface area that is electrochemically active. The downshift of the Pd d-band center, which weakens the binding energy of atoms, may contribute to the reduction of the active surface during alloy formation [43]. Based on the results of Fig. 5, we can conclude that the alloying of Pd metal with Mo lower d-band position of the top layer of Pd metal may have a significant impact on activity by producing straining and electron transfer between the substrate and over layer [44]. Electrochemically active surface area (ESA) determination is a reliable normalization technique that considers the active sites accessible for reaction. The theoretical charge required for this process (424 $\mu C/cm^2$) is divided by the experimental charge utilized to decrease a whole monolayer of Pd oxide in this method [45, 46]. For Pd/C and $PdMo_2/C$ nanocubes calculated, the ESA values were 6.3 m^2/g_{Pd} and 37.2 m^2/g_{Pd}, respectively.

Chronoamperometric Measurements

Chronoamperometric measurements are valuable methods for investigating the electrochemical activity and stability of catalysts in fuel cells [47, 48]. According to the chronoamperometry measurements performed on Pd/C and $PdMo_2/C$ catalysts, as shown in Fig. 6, the change in current values is very constant following a quick current decrease at the start. This indicates that the catalysts are stable. It is observed that the current values obtained for the $PdMo_2/C$ catalyst are much greater than the current values obtained for the Pd/C catalyst. A greater current density is a sign of increased electroactivity. This indicates that $PdMo_2/C$ is a more electroactive catalyst.

Impedance Measurements

The electrochemical impedance measurements were carried out using MEAs for the catalysts Pd/C and $PdMo_2/C$.

Fig. 4 EDX mapping imagines of **a** Pd/C and **b** $PdMo_2/C$

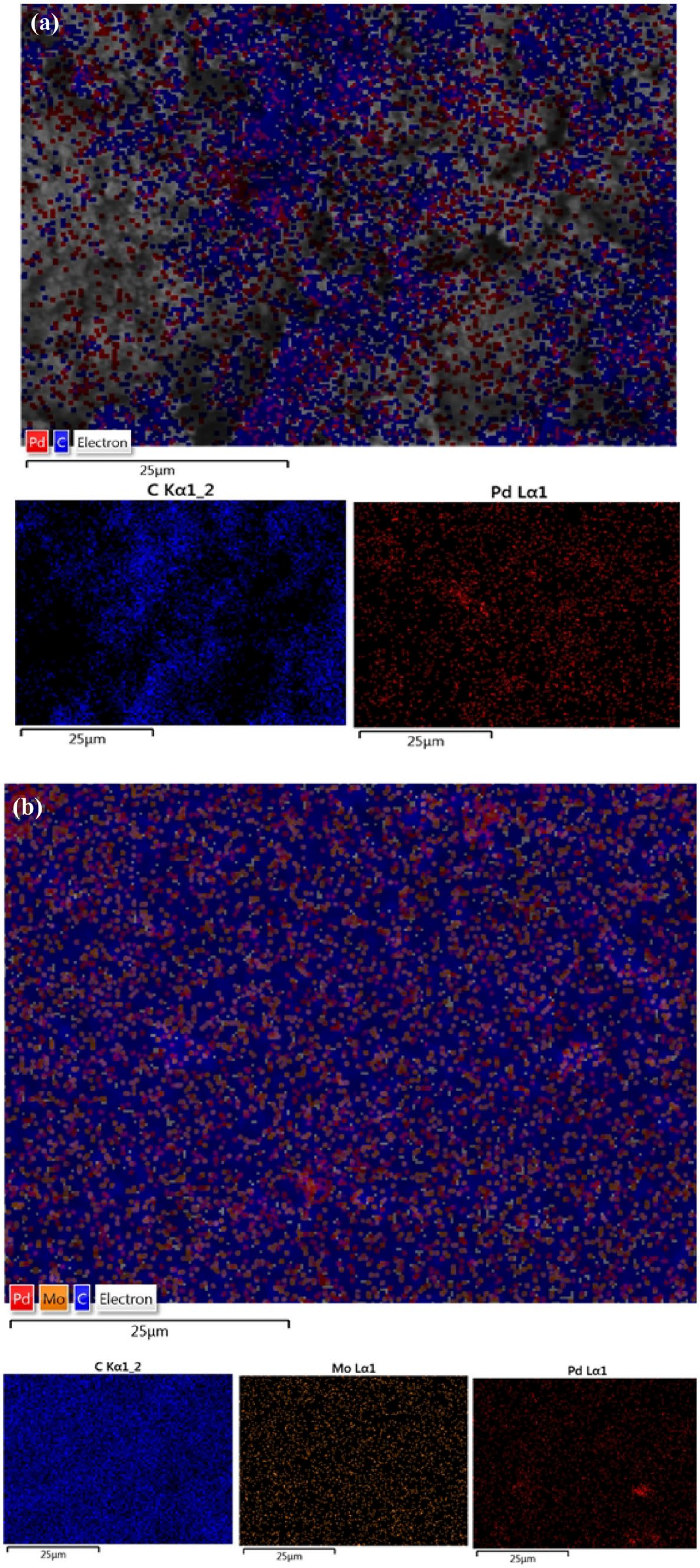

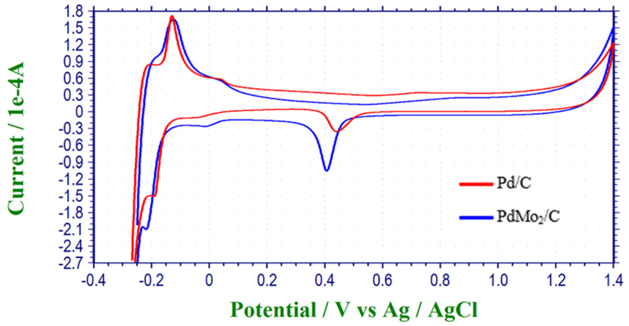

Fig. 5 Cyclic voltammograms of Pd/C and $PdMo_2/C$ catalysts in N_2 sat. 0.5 M H_2SO_4 at a scan rate of 50 $mVs.^{-1}$ (vs. Ag/AgCl)

Figure 7 shows the spectra of the single cells that used the two catalysts as cathode catalysts. Electrochemical impedance spectroscopy measurements show a partial semicircle in the high-frequency range of the Nyquist curves. Furthermore, it is shown the charge transfer resistance, and its diameter is based on the size of the charge transfer resistance. Since the electrochemical reaction rate is inversely proportional to the charge transfer resistance [49, 50], a low charge transfer resistance indicates high electrochemical activity. In Fig. 7, it is shown that since the diameter of the partial semicircle in the high-frequency zone produced for the electrode with the $PdMo_2/C$ catalyst is smaller than the diameter obtained for the Pd/C, the charge transfer resistance of the electrode with the $PdMo_2/C$ catalyst is lower. These suggest that the $PdMo_2/C$ catalyst has more significant electrochemical activity than the Pd/C catalyst, consistent with previous findings. The results of cyclic voltammetry and chronoamperometry are also consistent with this hypothesis. It may be attributed to the fact that increasing current density in the low polarization zone might accelerate the electrochemical kinetics of ORR [51].

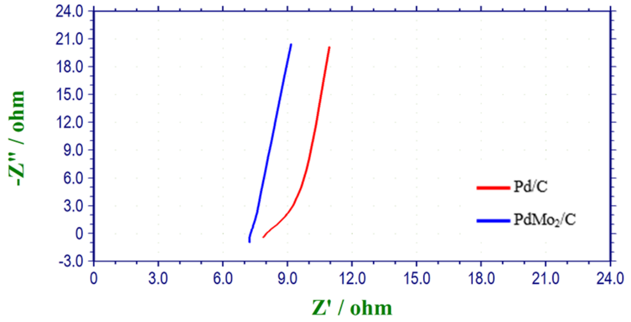

Fig. 7 Nyquist curves obtained from electrochemical impedance spectroscopy measurements of Pd/C and $PdMo_2/C$ catalysts in O_2 sat. 0.5 M H_2SO_4 solution

PEM Single Cell the ORR Activity Evaluation

Pd/C and atomic ratios PdMox/C electrocatalysts (1:x, $x = 1$, 2, and 3) were utilized as the cathode, while Pt/C was used as the anode membrane electrode assembly (MEA) was evaluated in a single PEM fuel cell test station. In addition, several atomic ratios of PdMo/C with comparable cathode loading were polarized to assess the performance and make comparisons. Figure 8 shows the polarization curves of Pd/C and different atomic ratios of PdMox/C cathodes at temperatures ranging from 40 to 70 °C. The performance of a single cell increased when the temperature of the cell was increased higher.

The open-circuit voltage decreased slightly as the Pd:Mo atom ratios increased. The reduction in OCV may be due to the effect of pore size on the electrode layer. That is, at a low Pd:Mo atomic ratio (high Mo content), it can cause a high degree of catalyst agglomeration with a low level of dispersion. However, it is clear that the different Pd:Mo atom ratios in the $PdMo_2/C$ electrocatalyst significantly affected cell performance in the activation region at high cell voltage

Fig. 6 Chronoamperometric curves of Pd/C and $PdMo_2/C$ catalysts in O_2 sat. 0.5 M H_2SO_4

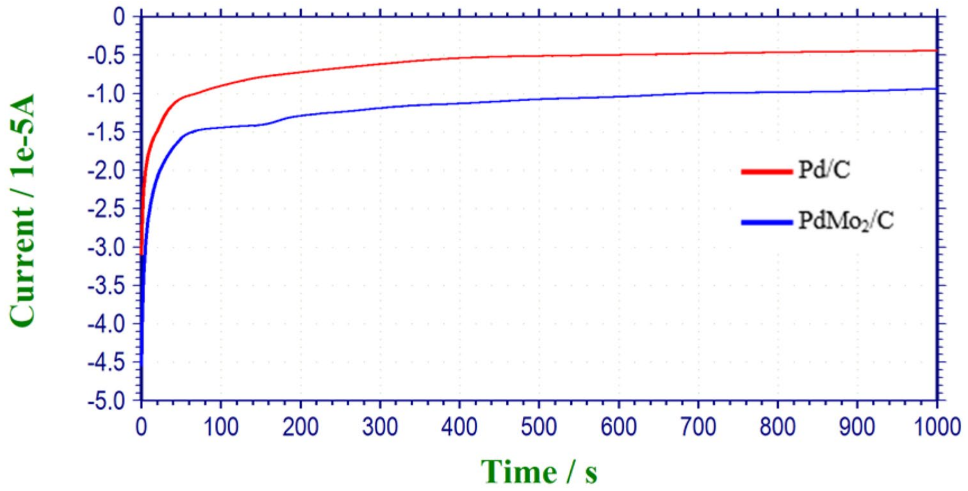

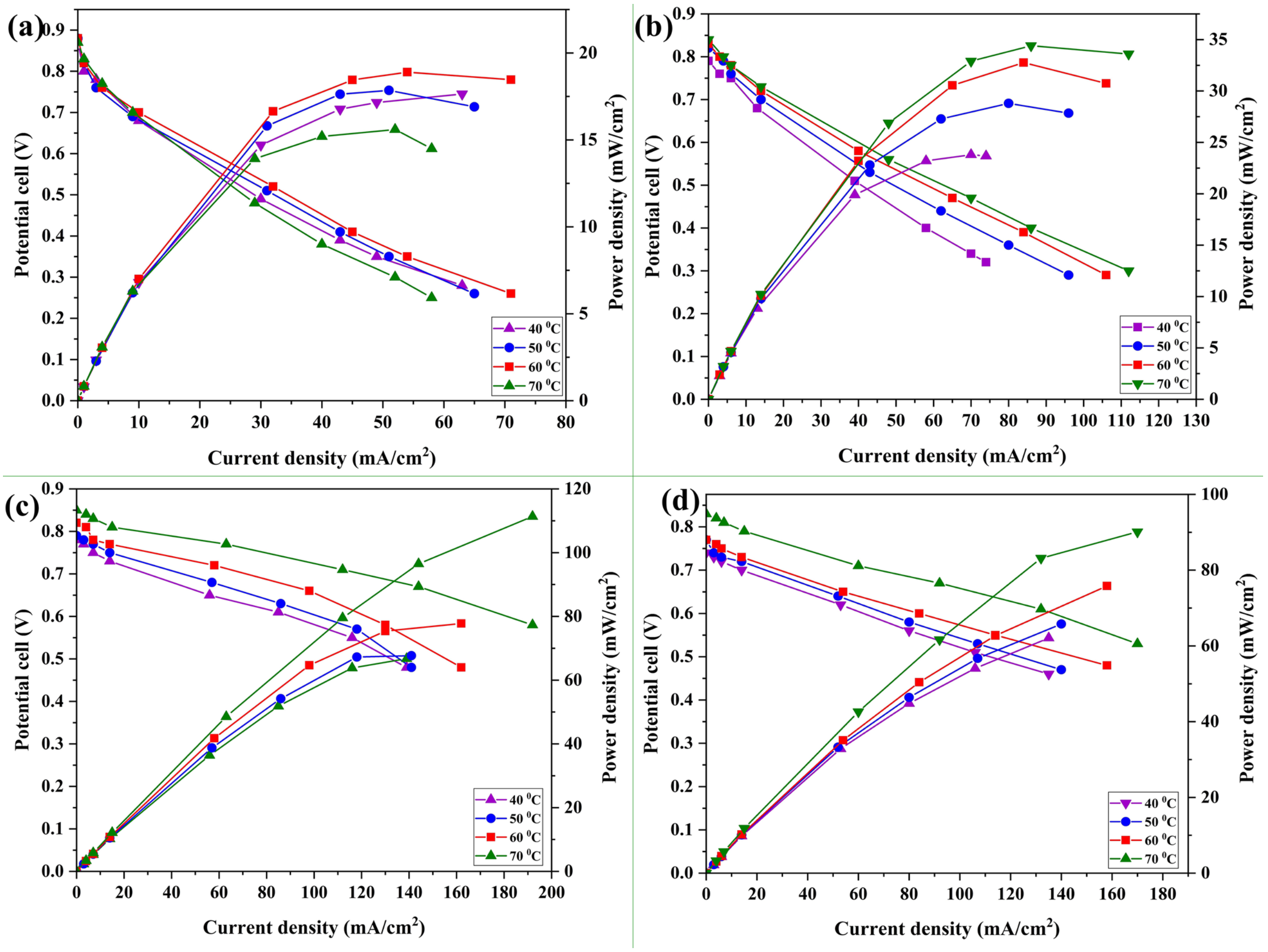

Fig. 8 Polarization curves **a** Pd/C, **b** PdMo/C, **c** $PdMo_2/C$, and **d** $PdMo_3/C$ electrocatalysts used as cathode with Pt/C as the anode. At ambient pressure, the cell was operated with humidified H_2/O_2 gas flow rate 20 mldk.$^{-1}$ at different temperatures (40 °C, 50 °C, 60 °C, and 70 °C)

and in the Ohmic region at medium to low cell voltages. This agglomeration causes a greater pore size to grow on the electrode layer, resulting in a more significant fuel crossover from the anode to the cathode and hence a lower OCV [52, 53]. Then, the oxygen reduction reaction (ORR) activity of the binary electrocatalyst may therefore be expressed in terms of the geometric surface area of the electrode by taking into account the influence of Pd:Mo atom ratios on cell performance in the activation-controlled region (the values of the current density at 0.83 V (j0.83 V) and the potential at 7 mA/cm^2).

In the polarization curve, it was observed that the performance of the PEM fuel cell with MEA containing PdMo/C (Pd:Mo = 1:2 ratio) was higher than the performance of the cell with Pd/C and various Pd:Mo atomic ratios under similar test circumstances (Fig. 9). The ORR activity of the Pd/C electrocatalyst appears to increase with increasing Mo content in the PdMo/C electrocatalyst. However, the best result is seen at Pd:Mo (1:2). Furthermore, when the polarization curve is examined, it is seen that the Ohmic losses and the concentration losses decrease when the atomic ratio of Mo in Pd increases by up to 2 mol. Therefore, it can be stated that increasing the Pd/C electrocatalyst property of Mo metal increases the ORR activity of MEA.

The efficiency of the as-synthesized catalysts was evaluated and compared at 70 °C cell temperature. Maximum current densities of synthesized catalysts at 70 °C cell temperature were measured as 61, 116, 188, and 168 mA cm^{-2} for Pd/C, PdMo/C, $PdMo_2/C$, and $PdMo_3/C$ catalysts, respectively. The efficiency according to the current of the $PdMo_2/C$ cathode catalyst at 70 °C was 52%, and Pd/C, PdMo/C, and $PdMo_3/C$ cathode catalysts at the same temperature were calculated as 26%, 38%, and 50%, respectively. Under the same conditions, the maximum power density was 107 mW cm^{-2} obtained for the $PdMo_2/C$ catalyst, while the Pd/C, PdMo/C, and $PdMo_3/C$ cathodes provided a maximum power density of 14.50, 33.60, and

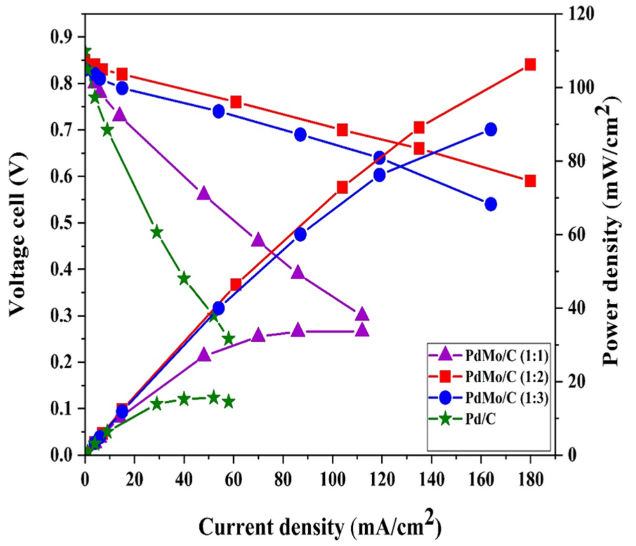

Fig. 9 Polarization curves of a single PEM fuel cell for ORR with Pd/C and different Pd:Mo atomic ratios, evaluated at 70 °C and ambient pressure. PdMox/C represents the Pd:Mo atomic ratio of 1:x (x = 1,2,3). Anode: 20 wt.% Pt/C, anode Pt loading: 0.15 mg(Pt) cm^{-2}. Cathode Pd loading: 0.15 mg(Pd) cm^{-2}, 0.13 mg(Pd) cm^{-2}, 0.096 mg(Pd) cm^{-2} versus 0.072 mg(Pd) cm^{-2}. H_2/O_2 flow rate: 20 mldk^{-1}. Membrane: Nafion 117

88.56 mWcm^{-2}, respectively. The ORR catalytic activity of as-synthesized electrocatalysts could be ordered as $PdMo_2/C > PdMo_3/C > PdMo/C > Pd/C$. The results of single-cell polarization reveal that Pd-decorated spinal have enhanced performance in the fuel cell by promoting the ORR process.

Conclusion

In this study, less costly carbon Vulcan XC-72-supported Pd and PdMo nanoparticles are synthesized by chemical reduction using sodium borohydride and formic acid methods as electro-catalysts in PEM fuel cells. Electrocatalysts made with different atomic ratios were used as cathode catalysts in PEM fuel cell applications at four different temperatures. The $PdMo_2$ electrocatalyst was found to be the most active cathode catalyst. The Pd/C and $PdMo_2/C$ catalysts exhibit diffraction peaks consistent with the face-centered cubic Pd structure at the appropriate locations in the X-ray patterns. The electrochemical results indicate that the $PdMo_2/C$ catalyst has a lower starting potential, a greater peak current density, and superior electrocatalytic activity than the Pd/C catalyst. A fuel cell test with a single cell also shows that the activity of the ORR increases with the temperature of the cell. The single-cell test calculated a maximum power density of 107 mWcm^{-2} with $PdMo_2/C$ as the cathode catalyst. The $PdMo_2/C$ catalyst has higher activity than Pd/C and other catalysts due to its smaller size and higher Mo content. Since the PdMo/C catalysts presented in this paper have good properties and are easy to make, we think it will lead to more research into cheaper electrocatalysts for PEM fuel cells under development.

Author Contribution Arzu Ekinci and Ömer Şahin contributed to the design and implementation of the research, to the analysis of the results, and to the writing of the manuscript. Abdurrahman Akdağ contributed to the analysis and interpretation of electrochemical measurements. Sabit Horoz contributed to the interpretation of the characterization studies of materials.

Funding The authors would like to express their gratitude to the Research Foundation of Siirt University for providing financial assistance via project 2021- SİÜSBF-10.

Data Availability Not applicable.

Declarations

Ethical Approval and Consent to Participate Not applicable.

Consent for Publication Informed consent was obtained prior to performing the procedure, including permission for publication of all photographs and images included herein.

Competing Interests The authors declare no competing interests.

References

1. Y. Wang, X. Wang, X. Wang, T. Liu, T. Zhu, S. Liu et al., Droplet dynamic characteristics on PEM fuel cell cathode gas diffusion layer with gradient pore size distribution. Renew. Energy. **178**, 864–874 (2021)
2. M. Çögenli, S. Mukerjee, A.B. Yurtcan, Membrane electrode assembly with ultra low platinum loading for cathode electrode of PEM fuel cell by using sputter deposition. Fuel Cells. **15**, 288–297 (2015)
3. S. Huo, W. Shi, R. Wang, B. Lu, Y. Wang, K. Jiao et al., Elucidating the operating behavior of PEM fuel cell with nickel foam as cathode flow field. Sci. China Technol. Sci. **64**, 1041–1056 (2021)
4. L. Lin, X. Zhang, H. Feng, X. Wang, Optimization of a serpentine flow field with variable channel heights and widths for PEM fuel cells. Sci. China Technol. Sci. **53**, 453–460 (2010)
5. J. Zhao, X. Li, A review of polymer electrolyte membrane fuel cell durability for vehicular applications: Degradation modes and experimental techniques. Energy Convers. Manage. **199**, 112022 (2019)
6. X. Lü, Y. Wu, J. Lian, Y. Zhang, C. Chen, P. Wang et al., Energy management of hybrid electric vehicles: A review of energy optimization of fuel cell hybrid power system based on genetic algorithm. Energy Convers. Manage. **205**, 112474 (2020)
7. H. Yang, W. Lee, B. Choi, Y. Ko, S. Yi, W. Kim, Self-humidifying Pt-C/Pt-TiO2 dual-catalyst electrode membrane assembly for proton-exchange membrane fuel cells. Energy. **120**, 12–19 (2017)
8. D. Fofana, S.K. Natarajan, J. Hamelin, P. Benard, Low platinum, high limiting current density of the PEMFC (proton exchange

membrane fuel cell) based on multilayer cathode catalyst approach. Energy. **64**, 398–403 (2014)

9. M. Sahoo, S. Ramaprabhu, Nitrogen and sulfur co-doped porous carbon–is an efficient electrocatalyst as platinum or a hoax for oxygen reduction reaction in acidic environment PEM fuel cell? Energy. **119**, 1075–1083 (2017)
10. Y. Tang, H. Zhang, H. Zhong, Y. Ma, A facile synthesis of Pd/C cathode electrocatalyst for proton exchange membrane fuel cells. Int. J. Hydrog. Energy. **36**, 725–731 (2011)
11. M. Shao, T. Huang, P. Liu, J. Zhang, K. Sasaki, M. Vukmirovic et al., Palladium monolayer and palladium alloy electrocatalysts for oxygen reduction. Langmuir. **22**, 10409–10415 (2006)
12. M.-H. Shao, K. Sasaki, R.R. Adzic, Pd− Fe nanoparticles as electrocatalysts for oxygen reduction. J. Am. Chem. Soc. **128**, 3526–3527 (2006)
13. J. Salvador-Pascual, S. Citalán-Cigarroa, O. Solorza-Feria, Kinetics of oxygen reduction reaction on nanosized Pd electrocatalyst in acid media. J. Power Sources. **172**, 229–234 (2007)
14. H. Li, G. Sun, Q. Jiang, M. Zhu, S. Sun, Q. Xin, Synthesis of highly dispersed Pd/C electro-catalyst with high activity for formic acid oxidation. Electrochem. Commun. **9**, 1410–1415 (2007)
15. J.L. Fernández, V. Raghuveer, A. Manthiram, A.J. Bard, Pd− Ti and Pd− Co− Au electrocatalysts as a replacement for platinum for oxygen reduction in proton exchange membrane fuel cells. J. Am. Chem. Soc. **127**, 13100–13101 (2005)
16. F. Fathirad, A. Mostafavi, D. Afzali, Bimetallic Pd–Mo nanoalloys supported on Vulcan XC-72R carbon as anode catalysts for direct alcohol fuel cell. Int. J. Hydrog. Energy. **42**, 3215–21 (2017)
17. H. Rostami, A.A. Rostami, A. Omrani, Investigation on ethanol electrooxidation via electrodeposited Pd–Co nanostructures supported on graphene oxide. Int. J. Hydrog. Energy **40**, 10596–10604 (2015)
18. H. Rostami, A. Omrani, A.A. Rostami, On the role of electrodeposited nanostructured Pd–Co alloy on Au for the electrocatalytic oxidation of glycerol in alkaline media. Int. J. Hydrog. Energy **40**, 9444–9451 (2015)
19. S. Shiva Kumar, S. Ramakrishna, D. Bhagawan, V. Himabindu, Preparation of RuxPd1-xO2 electrocatalysts for the oxygen evolution reaction (OER) in PEM water electrolysis. Ionics. **24**, 2411–2419 (2018)
20. S. Shiva Kumar, S. Ramakrishna, K. Naga Mahesh, B. Rama Devi, V. Himabindu, Palladium supported on phosphorus–nitrogen dual-doped carbon nanoparticles as cathode for hydrogen evolution in PEM water electrolyser. Ionics. **25**, 2615–2625 (2019)
21. D. Panjiara, H. Pramanik, Electrooxidation study of glycerol on synthesized anode electrocatalysts Pd/C and Pd-Pt/C in a Y-shaped membraneless air-breathing microfluidic fuel cell for power generation. Ionics. **26**, 2435–2452 (2020)
22. S.S. Kumar, N. Hidyatai, J.S. Herrero, S. Irusta, K. Scott, Efficient tuning of the Pt nano-particle mono-dispersion on Vulcan XC-72R by selective pre-treatment and electrochemical evaluation of hydrogen oxidation and oxygen reduction reactions. Int. J. Hydrog. Energy **36**, 5453–5465 (2011)
23. Y.-H. Qin, H.-H. Yang, X.-S. Zhang, X.-G. Zhou, L. Niu, W.-K. Yuan, Synthesis of highly dispersed and active palladium/carbon nanofiber catalyst for formic acid electrooxidation. J. Power Sources. **196**, 4609–4612 (2011)
24. A.B.A.A. Nassr, A. Quetschke, E. Koslowski, M. Bron, Electrocatalytic oxidation of formic acid on Pd/MWCNTs nanocatalysts prepared by the polyol method. Electrochim. Acta. **102**, 202–211 (2013)
25. N. Arul Dhas, H. Cohen, A. Gedanken, In situ preparation of amorphous carbon-activated palladium nanoparticles. J. Phys. Chem. B. **101**, 6834–6838 (1997)
26. Y. Xiong, J.M. McLellan, J. Chen, Y. Yin, Z.-Y. Li, Y. Xia, Kinetically controlled synthesis of triangular and hexagonal nanoplates of palladium and their SPR/SERS properties. J. Am. Chem. Soc. **127**, 17118–17127 (2005)
27. T. Teranishi, M. Miyake, Size control of palladium nanoparticles and their crystal structures. Chem. Mater. **10**, 594–600 (1998)
28. S. Chen, K. Huang, J.A. Stearns, Alkanethiolate-protected palladium nanoparticles. Chem. Mater. **12**, 540–547 (2000)
29. V. Mehta, J.S. Cooper, Review and analysis of PEM fuel cell design and manufacturing. J. Power Sources. **114**, 32–53 (2003)
30. X. Ding, S. Didari, T.F. Fuller, T.A. Harris, Membrane electrode assembly fabrication process for directly coating catalyzed gas diffusion layers. J. Electrochem. Soc. **159**, B746 (2012)
31. K. Mohanraju, P. Kirankumar, L. Cindrella, O.J. Kwon, Enhanced electrocatalytic activity of Pt decorated spinals (M3O4, M= Mn, Fe, Co)/C for oxygen reduction reaction in PEM fuel cell and their evaluation by hydrodynamic techniques. J. Electroanal. Chem. **794**, 164–174 (2017)
32. L. Cui, J. Zhang, H. Wang, S. Lu, Y. Xiang, The effects of different dimensional carbon additives on performance of PEMFC with low-Pt loading cathode catalytic layers. Int. J. Hydrog. Energy. **46**, 15887–15895 (2021)
33. G. Behmenyar, A.N. Akın, Investigation of carbon supported Pd–Cu nanoparticles as anode catalysts for direct borohydride fuel cell. J. Power Sources. **249**, 239–246 (2014)
34. L. Yi, W. Wei, C. Zhao, C. Yang, L. Tian, J. Liu et al., Electrochemical oxidation of sodium borohydride on carbon supported Pt-Zn nanoparticle bimetallic catalyst and its implications to direct borohydride-hydrogen peroxide fuel cell. Electrochim. Acta. **158**, 209–218 (2015)
35. J. Liu, L. Yi, X. Wang, Q. Zhao, Y. Zhang, J. Gao et al., Investigation of nanoporous carbon supported palladium–zinc nanocomposites as anode catalysts for direct borohydride–hydrogen peroxide fuel cell. Int. J. Hydrog. Energy. **40**, 7301–7307 (2015)
36. B. Jha, B. Mishra, B. Satpati, S. Ojha, Effect of thermal ageing on the evolution of microstructure and degradation of hardness of 2.25 Cr-1Mo steel. Mater. Sci. -Pol. **28**, 335 (2010)
37. R.D. Nikam, A.-Y. Lu, P.A. Sonawane, U.R. Kumar, K. Yadav, L.-J. Li et al., Three-dimensional heterostructures of MoS2 nanosheets on conducting MoO2 as an efficient electrocatalyst to enhance hydrogen evolution reaction. ACS Appl. Mater. Interfaces. **7**, 23328–23335 (2015)
38. M. Kempasiddaiah, V. Kandathil, R.B. Dateer, B. Sasidhar, S.A. Patil, S.A. Patil, Immobilizing biogenically synthesized palladium nanoparticles on cellulose support as a green and sustainable dip catalyst for cross-coupling reaction. Cellulose. **27**, 3335–3357 (2020)
39. M. Hara, U. Linke, T. Wandlowski, Preparation and electrochemical characterization of palladium single crystal electrodes in 0.1 M H2SO4 and HClO4: part I. Low-index phases. Electrochim. Acta. **52**, 5733–48 (2007)
40. S. Trasatti, O. Petrii, Real surface area measurements in electrochemistry. Pure Appl. Chem. **63**, 711–734 (1991)
41. M. Grdeń, M. Łukaszewski, G. Jerkiewicz, A. Czerwiński, Electrochemical behaviour of palladium electrode: Oxidation, electrodissolution and ionic adsorption. Electrochim. Acta. **53**, 7583–7598 (2008)
42. L.-I. Fang, Q. Tao, M.-F. Li, L.-W. Liao, D. Chen, Y.-X. Chen, Determination of the real surface area of palladium electrode. Chinese J. Chem. Phys. **23**, 543–548 (2010)
43. N. Kakati, J. Maiti, S. Lee, Y. Yoon, Core shell like behavior of PdMo nanoparticles on multiwall carbon nanotubes and their methanol oxidation activity in alkaline medium. Int. J. Hydrog. Energy. **37**, 19055–19064 (2012)
44. M. Shao, P. Liu, J. Zhang, R. Adzic, Origin of enhanced activity in palladium alloy electrocatalysts for oxygen reduction reaction. J. Phys. Chem. B. **111**, 6772–6775 (2007)

45. C. Jin, Z. Zhang, Z. Chen, Q. Chen, Effect of Ag modification on catalytic activity of Pd electrode for allyl alcohol oxidation in alkaline solution. Electrochim. Acta. **87**, 860–864 (2013)
46. W. Pan, X. Zhang, H. Ma, J. Zhang, Electrochemical synthesis, voltammetric behavior, and electrocatalytic activity of Pd nanoparticles. J. Phys. Chem. C. **112**, 2456–2461 (2008)
47. X. Liu, L. Yi, X. Wang, J. Su, Y. Song, J. Liu, Graphene supported platinum nanoparticles as anode electrocatalyst for direct borohydride fuel cell. Int. J. Hydrog. Energy. **37**, 17984–17991 (2012)
48. S. Eris, Z. Daşdelen, F. Sen, Enhanced electrocatalytic activity and stability of monodisperse Pt nanocomposites for direct methanol fuel cells. J. Colloid Interface Sci. **513**, 767–773 (2018)
49. M.H. Atwan, C.L. Macdonald, D.O. Northwood, E.L. Gyenge, Colloidal Au and Au-alloy catalysts for direct borohydride fuel cells: electrocatalysis and fuel cell performance. J. Power Sources. **158**, 36–44 (2006)
50. Y. Zhang, Y. Hu, S. Li, J. Sun, B. Hou, Manganese dioxide-coated carbon nanotubes as an improved cathodic catalyst for oxygen reduction in a microbial fuel cell. J. Power Sources. **196**, 9284–9289 (2011)
51. Z. Xie, S. Holdcroft, Polarization-dependent mass transport parameters for orr in perfluorosulfonic acid ionomer membranes: an EIS study using microelectrodes. J. Electroanal. Chem. **568**, 247–260 (2004)
52. Thanasilp S, Hunsom M. Effect of Pt: Pd atomic ratio in PtePd/C electrocatalyst-coated membrane on the electrocatalytic activity of ORR in PEM fuel cells. Renew. Energy. (2011)
53. J. Li, F. Ye, L. Chen, T. Wang, J. Li, X. Wang, Correlation of electrochemical and physical properties of PtRu alloy electrocatalysts for PEM fuel cells. J Power Sources. **186**, 320 (2009)